Title

Femtosecond Extreme Ultraviolet Photoemission Spectroscopy: Observation of Ultrafast Charge Transfer at the n-TiO2/p-Si(100) Interface with Controlled TiO2 Oxygen Vacancies

Journal

The Journal of Physical Chemistry C, 120(5)

ISSN

1932-7447

Authors

Vaida, Mihai E

Leone, Stephen R

Publication Date

2016-02-11

DOI

10.1021/acs.jpcc.5b11161

Peer reviewed

THE JOURNAL OF PHYSICAL CHEMISTRY C

Article

pubs.acs.org/JPCC

Femtosecond Extreme Ultraviolet Photoemission Spectroscopy: Observation of Ultrafast Charge Transfer at the n-TiO_2/p-Si(100) Interface with Controlled TiO_2 Oxygen Vacancies

Mihai E. Vaida[†] and Stephen R. Leone*[,†,‡,§]

[†]Department of Chemistry and [‡]Department of Physics, University of California, Berkeley, California 94720, United States

[§]Chemical Sciences Division, Lawrence Berkeley National Laboratory, Berkeley, California 94720,United States

ABSTRACT: Wide band gap heterostructures can be accurately fabricated at room temperature to exhibit remarkable electrical properties that facilitate the transfer of electrons across the heterojunction while blocking the transfer of holes. The present investigation focuses on engineering the electronic structure of a TiO_2 overlayer on a p-type doped Si(100) substrate by controlling the concentration of TiO_2 oxygen vacancies. TiO_2 films are deposited on p-Si(100) in an ultrahigh vacuum setup by evaporation of Ti atoms at a constant rate in a variable O_2 atmosphere. The concentration of oxygen vacancies and consequently the degree of n-type doping of TiO_2 is tuned by controlling the oxygen background pressure during the TiO_2 formation. To investigate the electronic structure and the concentration of defects in the TiO_2 layer as well as to characterize the TiO_2/p-Si(100) band alignment we used photoelectron spectroscopy employing femtosecond extreme ultraviolet laser pulses produced via high harmonic generation. Furthermore, using a pump−probe technique in conjunction with photoemission spectroscopy, an ultrafast electron injection from the p-Si(100) substrate into the defect-rich TiO_2 layer is observed with a time constant of 450 fs, as well as the subsequent charge carrier recombination. The latter is revealed to be affected by the oxygen defects when investigated with femtosecond resolution. No charge transfer is observed when defect-poor TiO_2 films are prepared on the p-Si(100) substrate. This might be attributed to a change in the energy band alignment at the TiO_2/Si(100) interface that reduces the built-in potential across the heterojunction and consequently reduces the driving force responsible for the injection of electrons into the TiO_2 layer.

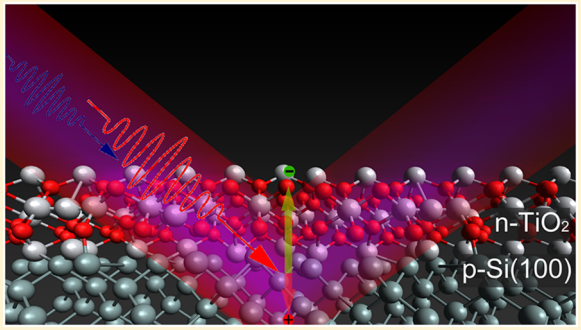

1. INTRODUCTION

After photoexcitation, the spatial separation of electrons and holes is a key factor that impacts the efficiency of solar cells and photocatalytic materials.[1] In the particular case of conventional solid-state solar cells, p−n junctions are widely used as photovoltaic materials.[2] Their fabrication costs are relatively high, because they require high-purity materials, ultra clean tools, and processing at elevated temperatures.[3] Recently, it has been demonstrated that solar cells based on TiO_2/Si heterojunctions with a power conversion efficiency greater than 7% can be fairly simply and inexpensively fabricated.[4] Both Si[5] and TiO_2[6] are abundant, inexpensive, nontoxic, and easy to handle semiconductors. TiO_2 films grown on Si form a staggered heterojunction (type II) that exhibits remarkable electrical properties, allowing a selective separation of charges. Due to the small difference between the conduction band minima of Si and TiO_2, the photogenerated electrons in Si can easily migrate to TiO_2. However, the large difference between the valence band maxima of these semiconductors prevents the migration of holes from Si to TiO_2.

Although the selective charge transfer from Si to TiO_2 has been demonstrated,[4] the factors that can impact the power conversion efficiency of the photovoltaic TiO_2/Si heterojunction, e.g., charge-carrier recombination due to defect states, have not been investigated thus far. In this work, femtosecond (fs) extreme ultraviolet (XUV) laser pulses in conjunction with photoemission spectroscopy are used to investigate the electronic structure of ultrathin TiO_2 films on a p-Si(100) substrate. The femtosecond pump−probe technique allows time-resolved investigation of the electronic structure and reveals the critical time constants that characterize the charge transfer at the surface of the material. Moreover, because the photoelectrons probed with femtosecond-XUV laser pulses cannot travel through more than 2−3 monolayers (ML) of solid materials,[7] the photoemission technique also offers high surface sensitivity.

The present work is focused on investigating the electronic structure of ultrathin TiO_2 films grown on p-Si(100) and measures how the relative shifts of the valence band energies and electron transfer rates are affected by the TiO_2 degree of oxidation. Furthermore, electron injection from the p-Si(100) substrate to the ultrathin TiO_2 film and the impact of the defect

Received: November 14, 2015
Revised: December 29, 2015
Published: January 20, 2016

DOI: 10.1021/acs.jpcc.5b11161
J. Phys. Chem. C 2016, 120, 2769−2776

states of TiO_2 on the charge recombination is monitored with femtosecond resolution by monitoring the ultrafast negative charging of TiO_2.

2. EXPERIMENTAL SETUP

A new experimental setup that will be described in detail elsewhere is employed to prepare and characterize TiO_2 films on a p-Si(100) substrate as well as to investigate the ultrafast photoinduced charge transfer at the n-TiO_2/p-Si(100) interface. Briefly, the experimental setup consists of two main parts: (i) the femtosecond laser system in conjunction with a pump−probe setup that includes a high-order harmonics generation (HHG) source and a monochromator and (ii) an ultrahigh vacuum (UHV) surface science chamber. The femtosecond laser light is produced with a Ti:sapphire oscillator continuously pumped by a 6 W frequency-doubled Nd:YVO_4 laser. The laser pulses are amplified with a Nd:YLF laser pumped Ti:sapphire amplifier to yield 24 fs pulses in the infrared (IR) spectral domain, at a central wavelength of 800 nm, a typical power of 2.2 W, and a repetition rate of 1 kHz. The amplified laser beam is divided into two arms to produce the pump and the probe laser beams. In the present investigation, the fundamental wavelength, i.e., 800 nm, is used as a pump pulse. The probe pulse is produced via high harmonic generation (HHG) in rare gases. The high harmonic source and the monochromator used in this work are similar to one used in our laboratory for gas-phase investigations[8] but provide a better temporal resolution, a broader range of harmonics, and UHV compatibility.

For the HHG process, the laser beam at 800 nm is focused to 10^{14}−10^{15} W cm^{-2} at the exit of a semi-infinite gas cell filled with Ar at 25 Torr. Odd harmonics ranging from the 7th to 29th order are produced. To obtain a single harmonic, the high-harmonics beam is dispersed by a plane grating in first-order diffraction at grazing incidence. Subsequently, the high-harmonics beam is focused on the sample surface inside the UHV chamber by a combination of a cylindrical and a toroidal mirror to a spot size of about 0.2 mm. A slit mounted at the laser beam entrance of the UHV chamber allows a single harmonic to enter the UHV chamber and blocks all the other harmonics. This slit also allows an efficient differential pumping of the vacuum apparatus. The pump and the probe laser beams are overlapped on the sample surface by an aluminum mirror installed inside the vacuum apparatus a few millimeters above the XUV laser beam. For the present investigation, only the 27th harmonic (41.85 eV) with a spectral width of about 1 eV is used.

The IR-pump laser beam is passed through a computer-controlled optical delay stage. When the delay stage is moved, the optical path of the pump beam is varied, changing the time delay between the pump and the probe pulses. To determine the zero time delay between the pump and probe laser pulses, the plane grating of the monochromator is rotated to the zero diffraction order so that IR laser beam that produces the HH is directed onto the surface and overlapped with the IR-pump laser beam. The zero time delay is subsequently obtained from the peak maximum of the integral transient photoemission produced by both IR pump and probe laser beams. The same result is obtained with the IR-pump and XUV-probe laser beams from a molybdenum surface using the laser-assisted photoelectric effect (LAPE) reported by Saathoff et al.[9] Based on the LAPE and other transient surface photovoltage measurements, an instrumental time response function of about 80 fs is obtained, which is shorter than the duration of the processes measured in the present experiment.

The UHV surface science chamber contains specific tools for surface preparation and characterization such as an Ar ion gun for surface cleaning, a Ti oven used for the preparation of Ti and TiO_2 films, and an Auger electron spectrometer to investigate the surface composition and cleanliness. A time-of-flight photoelectron spectrometer (TOF-PES), consisting of a 1 m long, double wall mu-metal tube, is employed to investigate the surface electronic structure. Electron detection is accomplished by a microchannel-plate amplifier in conjunction with a 5 GHz multichannel scaler electronics unit for data acquisition. During the photoemission experiments, the sample surface is positioned 5 mm from the TOF-PES entrance with the surface normal parallel to the spectrometer axis. A negative bias of typically 5−10 V is applied to the surface to prevent cutting off the low-energy electrons due to the work function difference between the substrate and the spectrometer. The laser beam incidence angle is 45°.

The sample surface is attached to a liquid nitrogen cryostat, which is mounted in the center of the UHV chamber. The surface sample−cryostat assembly can be vertically translated and horizontally rotated by 360° via a mechanical manipulator. Furthermore, an *xy*-horizontal translation stage allows movement of the assembly by ±12 mm from the midpoint. The crystal position can be reproduced with an accuracy greater than 0.02 mm and 0.5°.

The base pressure of the UHV surface science chamber is 1.5×10^{-10} Torr. During the XUV photoemission experiments, the pressure in the UHV chamber rises to 2.0×10^{-10} Torr due to the residual Ar gas originating from the HHG source.

3. RESULTS AND DISCUSSION

3.1. Preparation of TiO_2 on Si(100). For the present investigations, a p-doped Si(100) substrate with a resistivity of 100 Ω·cm is used. The clean Si(100) surface is prepared by several cycles of Ar^+ sputtering (0.5 keV, 7 μA) for 20 min followed by 5 min of annealing at 600 K until no oxygen, carbon, or other contaminates are observed in Auger electron spectroscopy (AES) (Figure 1a).

For the preparation of the TiO_2 films, a home-built Ti metal evaporator that contains a Ti filament with purity of 99.99% is employed. The TiO_2 ultrathin films are synthesized by evaporation of Ti metal in an oxygen atmosphere on the Si(100) substrate held at room temperature. An Auger electron spectrum recorded after the deposition of 3 ML TiO_2 on Si(100) is shown in Figure 1b. This spectrum shows that the Si_{LVV} peak at 91 eV decreases after TiO_2 deposition while new Auger transitions specific for oxygen and titanium appear, i.e., Ti_{LMM} at 385 eV, Ti_{LMV} at 417 eV, and O_{KLL} at 510 eV.

Auger electron spectroscopy is also employed in the investigations to calibrate the Ti deposition rate from the oven and subsequently the TiO_2 film thickness. The inset in Figure 1 shows the Ti/Si AES ratio as a function of the Ti evaporation time. A gradual increase of the Ti evaporation time on the Si(100) surface leads to a break-point in the intensity ratio of the Ti_{LMM} AES signal at 385 eV to the Si_{LVV} AES signal at 91 eV, which corresponds to the amount of Ti needed for the completion of the first Ti layer on Si(100). The resulting Ti evaporation rate is determined to be 0.35 ML/min.

3.2. XUV Photoemission Spectroscopy. In general, to study the oxidation of a metal surface under UHV conditions, the AES technique is employed.[10] A previous report using the

DOI: 10.1021/acs.jpcc.5b11161
J. Phys. Chem. C 2016, 120, 2769−2776

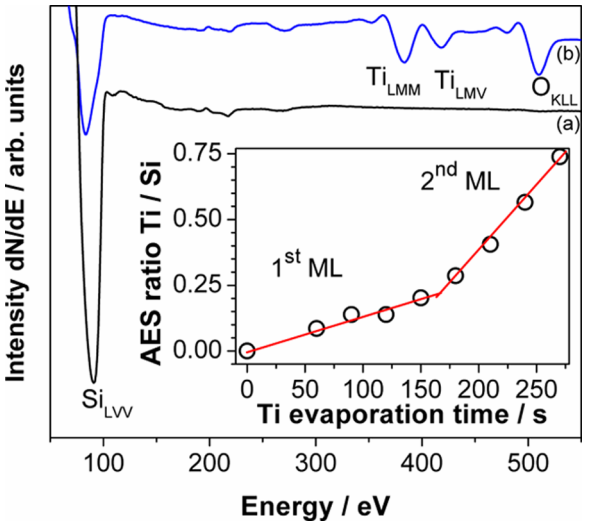

Figure 1. Auger electron spectra recorded from (a) Si(100) surface and (b) 3 ML Ti evaporated on Si(100) in oxygen atmosphere (5×10^{-7} Torr O_2). The inset shows the Ti to Si(100) Auger electron intensity ratio as a function of Ti deposition time. The break point in the AES ratio plot corresponds very closely to the initial appearance of the TiO_2 second layer.

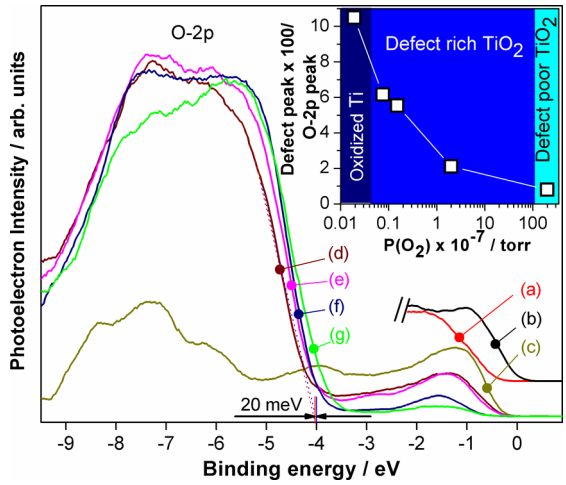

Figure 2. Photoemission spectra recorded with the 27th harmonic from (a) p-Si(100) substrate, (b) 3 ML Ti on p-Si(100), and 3 ML Ti evaporated on p-Si(100) at room temperature and various O_2 background pressures: (c) 1×10^{-9} Torr, (d) 7.5×10^{-9} Torr, (e) 1.5×10^{-8} Torr, and (f) 2×10^{-7} Torr. (g) Photoemission spectrum of 3 ML of Ti evaporated on p-Si(100) at 575 K and an O_2 background pressures of 2×10^{-5} Torr. The linear extrapolation of the O-2p rising edge (dotted lines) used for the determination of the VBM as well as the error of 0.02 eV in the determination of the VBM are displayed, as an example, for one of the photoemission spectra. The inset shows the percentage value of the surface area of the defect peak relative to the area of the O-2p photoemission peak obtained in the case of the low-defect TiO_2 film obtained at an O_2 background pressure of 2×10^{-5} Torr (g).

AES method investigated the satellite features of the Ti_{LMM} transition to study the formation of TiO_2 and to gain insight about the titanium degree of oxidation.[11] AES investigations were also performed in our laboratory to investigate the TiO_2 formation. However, we observed that the XUV-photoemission spectroscopy technique is much more sensitive than AES to the electronic structure changes that occur during the Ti oxidation, which is discussed in more detail here. As described below, XUV-photoemission spectroscopy is able not only to investigate the formation of TiO_2 but also to detect the defect electronic states in the TiO_2 band gap and to estimate their density. Moreover, the XUV-photoemission measurements are also able to establish information about the band alignments and energies for defect-rich and defect-poor TiO_2 films attached to silicon, when coupled with existing data in the literature.

Figure 2 displays the valence band photoemission spectra recorded with the 27th harmonic of the p-Si(100) substrate, of a 3 ML Ti film grown on p-Si(100) without oxygen admission, and of 3 ML Ti films evaporated on p-Si(100) at various O_2 background pressures. The binding energy in Figure 2 is referenced to the Fermi level ($E_F = 0$), which is determined from the photoemission onset of the Ta clips that hold the Si(100) substrate and from the Ti layer evaporated on p-Si(100) (cf. Figure 2b). The photoemission spectrum obtained from the p-Si(100) substrate in the binding energy region of 0 eV to −2 eV is shown in Figure 2a. The valence band maximum (VBM) of the p-Si(100) substrate, which is −0.40 eV below the E_F, is determined as the intersection point where the extrapolation of the linear portion of the Si(100) rising edge intersects the straight line describing the background.[12] After the evaporation of 3 ML Ti on p-Si(100) at room temperature at a pressure of 2×10^{-10} Torr, the onset of the photoemission spectrum shifts to E_F (0 eV binding energy), which is characteristic for photoelectrons originating from a metal electronic structure (cf. Figure 2b). When 3 ML of Ti is evaporated on p-Si(100) at room temperature in an O_2 atmosphere of 1×10^{-9} Torr, the photoemission spectrum further changes (cf. Figure 2c). The photoemission onset shifts to −0.36 eV below E_F, and an intense peak at low binding energies with a maximum at −1.2 eV appears. Moreover, a photoemission feature becomes visible between −5.5 and −9.5 eV. Increasing the O_2 background pressure to 7.5×10^{-9} Torr leads to further major changes of the photoemission spectrum (cf. Figure 2d). The photoemission onset slightly shifts to higher binding energy, and the peak at low binding energies decreases in intensity and shifts its maximum at −1.38 eV while a broad photoemission feature that appears as a double-peak structure with maxima at −5.5 and −7.5 eV becomes apparent. Further increasing the O_2 background pressure to 1.5×10^{-8} and 2×10^{-7} Torr during Ti evaporation at room temperature leads to a decrease of the photoemission intensity of the peak at low binding energies as well as a shift of this peak maximum toward higher binding energies (cf. Figure 2e,f). In addition, the broad, double-peak structure photoemission feature shifts to lower binding energy with increasing O_2 background pressures. There are no further significant changes in the photoemission spectrum if the O_2 background pressure is increased by another order of magnitude. However, a considerable decrease of the peak at low binding energies is obtained when Ti is evaporated at higher substrate temperatures. Figure 2g displays a photoemission spectrum of Ti evaporated on the p-Si(100) substrate held at 575 K in an O_2 background pressure of 2×10^{-5} Torr. The TiO_2 preparation at elevated substrate temperatures leads to fully oxidized films.[13]

The photoemission spectra obtained from Ti evaporated on Si(100) in O_2 background pressures higher than 7.5×10^{-9} Torr resemble the main features obtained in previous photoemission investigations of TiO_2.[14] The photoemission peak that shifts from −1.22 to −1.7 eV and diminishes as the

DOI: 10.1021/acs.jpcc.5b11161
J. Phys. Chem. C 2016, 120, 2769−2776

O_2 background pressure is increased during Ti evaporation is attributed to defect states, i.e., occupied electronic states located within the band gap of TiO_2. These defects are derived from Ti-3d states as a result of oxygen vacancies resulting in the formation of $Ti^{3+}(d^1)$.[14] Pacchioni and co-workers investigated by means of density functional theory (DFT) the electronic structure in the bulk of anatase TiO_2 containing oxygen vacancies.[15] They found that the defect states in the band gap of TiO_2 are located between 2.60 and 2.88 eV above the VBM, which perfectly matches the energy location of the defect photoemission peak observed in the present experiments. Consequently, in our investigations, the intensity of the photoemission peak observed in the band gap of TiO_2 is directly connected to the density of defect states. The broad double-peak structure photoemission feature is due to the O-2p states that make up the valence band of TiO_2. Thus, the states at −5.5 eV are assigned to the Ti-3d−O-2p π-bonding states while the peak at −7.25 eV is assigned to the O-2p−Ti-3d σ-bonding states.[14]

Based on the previous discussion, the photoemission spectra shown in Figure 2, and the literature reports,[14,15] as Ti is evaporated on Si(100) at various background O_2 pressures, four situations are distinguished. (i) Ti evaporation without O_2 admission leads to the formation of a Ti layer, and the photoemission onset in this case coincides with the E_F. (ii) The evaporation of Ti at an O_2 background pressure of 1×10^{-9} Torr leads to the formation of a minimally oxidized Ti layer. In this case, the photoemission spectrum is different than the one obtained from a Ti or a TiO_2 surface, i.e., the photoemission onset is below E_F and there is a low density of states at binding energies between −5.5 and −9.5 eV, which indicates that the valence band of TiO_2 is not formed yet. (iii) When Ti is evaporated on Si(100) at an O_2 background pressure of 7.5×10^{-9} Torr, a defect-rich TiO_2 film is formed. In this case, the intense photoemission at binding energies between −5.5 and −9.5 eV indicates the formation of the O-2p states and hence the formation of the TiO_2 valence band. Moreover, the photoemission from the occupied states in the band gap of TiO_2 indicates the existence of a defect-rich TiO_2 layer. Further increases in the O_2 background pressure lead to better-oxidized films and consequently fewer defect states in the band gap of TiO_2. (iv) A defect-poor TiO_2 film is obtained when Ti is evaporated on Si(100) at 575 K at an O_2 background pressure higher than 2×10^{-5} Torr.

If it is assumed that the photoemission cross section does not change significantly as a function of energy in the spectral range shown in Figure 2, an estimate of the density of states (DOS) in the band gap of the TiO_2 films relative to the O-2p DOS as a function of O_2 background pressure can be performed. The inset in Figure 2 displays the percentage value of the photoemission surface area in the binding energy region from 0 to −3.5 eV relative to the area of the defect-poor O-2p peak (cf. spectrum g in Figure 2) as a function of O_2 background pressure. As can be observed in the inset of Figure 2, the DOS within the band gap of TiO_2 films can be precisely tuned and varied from 0.07% to 6% relative to the O-2p DOS by controlling the O_2 background pressure during the Ti evaporation.

Another feature that is observed in the TiO_2 spectra displayed in Figure 2 is the shift of the O-2p rising edge as a function of the O_2 background pressure. The VBM of TiO_2 is determined from the extrapolation of the linear portion of the O-2p rising edge as explained above for the case of Si(100). The VBM of the defect-poor TiO_2 is −3.65 ± 0.02 eV while for the defect-rich it shifts to −4.00 ± 0.02 eV. The error of ±0.02 eV in the determination of the VBM is due to inaccuracy in the extrapolation of the linear portion of the O-2p rising edge. Based on the photoemission spectra displayed in Figure 2, both the defect-rich and defect-poor TiO_2 films investigated in this work are n-type doped, because E_F is located close to the CBM, i.e., E_F is 0.6 and 0.95 eV below the CBM of TiO_2 for defect-rich and defect-poor films, respectively. The shift of the VBM toward higher binding energies when the density of defects in TiO_2 is increased indicates that the defect-rich TiO_2 is more n-type doped than the defect-poor TiO_2. This result is in agreement with the previous investigations by Onda et al.,[16] which show that the TiO_2 becomes n-type doped after generation of oxygen vacancies. Consequently, the concentration of oxygen vacancies and the degree of n-type doping of TiO_2 can be tuned by controlling the oxygen background pressure during the TiO_2 formation.

The experimental setup used in this investigation does not contain tools to measure the energy of the conduction band minimum (CBM); hence, a direct determination of the TiO_2 band gap is not possible. Nevertheless, similar investigations performed by Jhaveri et al.,[17] in which ultrathin TiO_2 films of 1−4 nm are deposited on Si substrates, have found the VBM of TiO_2 located at 3.8 eV below E_F and measured a band gap of 4.6 eV. DFT investigations also found that the band gap of anatase-TiO_2 containing oxygen vacancies is 3.9 and 4.4 eV at the Γ and X points, respectively.[15] These energy values of the band gap are in perfect agreement with the present investigation. Previously reported values of the TiO_2 band gap range from 3.0 to 3.8 eV depending on crystal structure and preparation method, which are smaller than the one obtained by Jhaveri et al. for an ultrathin TiO_2 film on Si.[17] Jhaveri et al. attribute this discrepancy to the fact that the electronic structure of ultrathin films is different than the electronic structure of thicker TiO_2 samples previously investigated by other researchers.

Figure 3 displays a tentative energy band diagram of the defect-poor and defect-rich n-TiO_2/p-Si(100). The energy band alignments are constructed using the VBM energies of p-Si(100), and of defect-poor and defect-rich n-TiO_2 measured in this work, the band gap energy of ultrathin TiO_2 films reported by Jhaveri et al.,[17] and the literature value of the Si band gap.[18] For a defect-rich n-TiO_2/p-Si(100) sample, the CBM of p-Si(100) is higher than the CBM of TiO_2 by 0.15 ± 0.02 eV, while in the case of defect-poor n-TiO_2 on p-Si(100) the CBM of p-Si(100) is lower than the CBM of TiO_2 by 0.20 ± 0.02 eV. In the energy band diagrams displayed in Figure 3 it is considered that the band gap energy of TiO_2 does not change with the defect density, and the band gap energy just shifts by 0.35 ± 0.02 eV as observed in the photoemission spectra shown in Figure 2. However, the band gap energy of TiO_2 might change as the defect states are formed.

The band banding at the n-TiO_2/p-Si heterojunction displayed in Figure 3 indicates the formation of a space charge region at the interface, across which a gradient of free charge carriers occurs. Such a space charge region usually forms when n- and p-type semiconductors are coupled to form a junction.[19] The gradient of free charge carriers across the space charge region leads to the formation of a built-in electric field.[19a] In general, photoexcited charge carriers at the n−p heterojunction are separated by this built-in electric field, electrons being accelerated toward the n-type semiconductor, and the holes

DOI: 10.1021/acs.jpcc.5b11161
J. Phys. Chem. C 2016, 120, 2769−2776

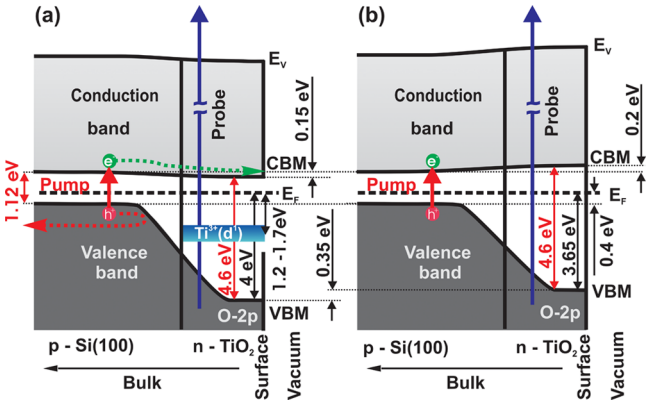

Figure 3. Schematic energy level diagram illustrating the band alignment of (a) defect-rich and (b) defect-poor n-TiO_2/p-Si(100) and the assignment of the different excitation processes that lead to the observed transient photoemission signals of Figure 4. The energy values measured in the present investigation are written in black while the literature values are written in red. The red and blue arrows represent the IR-pump and XUV-probe laser pulses, respectively. The dashed curved arrows represent the possible trajectories of the charged carriers. The $Ti^{3+}(d^1)$ defect states in the band gap of defect-rich n-TiO_2 are represented by a blue rectangle.

toward the p-type semiconductor.[20] The built-in electric field across the TiO_2/Si heterojunction can inject photoexcited electrons from the p-Si(100) substrate into the n-TiO_2 layer. To explore this further, the photoinduced charge separation and migration at the TiO_2/Si heterojunction can be investigated in the present experiment using the pump−probe photoemission technique.

3.3. Ultrafast Charge Transfer Across the n-TiO_2/p-Si(100) Heterojunction. As mentioned above, previous investigations on TiO_2/Si heterojunctions demonstrated that electrons excited in Si can migrate into the TiO_2, while the hole migration from Si to TiO_2 is prevented because of the large hole-barrier at the interface.[4a,17] This charge transfer across the TiO_2/Si(100) heterojunction has not been investigated with femtosecond resolution thus far. Therefore, to gain insights into the time scale of this charge transfer, defect-rich and defect-poor TiO_2 films with a thickness of 3 ML were prepared in UHV on p-Si(100). The TiO_2 film thickness was chosen to be 3 ML for a number of reasons. (i) A 3 ML film is much thinner than the space charge region that is formed at the surface of a doped semiconductor, i.e., tens of nanometers or more; therefore, in the present experiment (ii) the effect of a charge injected from the Si(100) substrate into the 3 ML TiO_2 film can be considered to be already at the TiO_2/vacuum interface. Its effect would be easily detected via XUV-photoemission spectroscopy, because the mean free path of the photoelectrons created with the XUV-probe laser pulse in our experiment is 1−3 ML.[7] (iii) Moreover, the electronic structure of a 3 ML TiO_2 film resembles the main features of the TiO_2 bulk, i.e., the energetic location of the Ti-3d−O-2p π-bonding, O-2p−Ti-3d σ-bonding, and $Ti^{3+}(d^1)$ states. However, the band gap energy measured in the present experiment from the 3 ML TiO_2 is slightly larger than the value measured for bulk TiO_2. Our result is in agreement with other investigations performed on ultrathin metal oxide films, which show that the electronic structure of a 3 ML film resembles the main characteristic of the bulk material.[16]

To investigate the time-resolved charge carrier dynamics at the TiO_2/Si(100) interface, the following pump−probe schema is employed. The IR-pump laser pulse at the central wavelength of 800 nm (1.55 eV) is used to excite electrons from the valence band into the conduction band of p-Si(100), leaving holes in the valence band. Subsequently, the photogenerated electrons and holes will separate in the space charge region at the n-TiO_2/p-Si(100) heterojunction by the built-in electric field. The electrons are accelerated toward the n-TiO_2 while the holes are accelerated toward the bulk of the p-Si(100) substrate. The electrons that migrate across the heterojunction will slightly negatively charge the TiO_2 ultrathin film and consequently the surface of the sample. The excess electrons at the surface will act as a small negative bias potential applied on the sample that will increase the kinetic energy of the photoelectrons ejected from the surface. Subsequently, the XUV-probe laser pulse that produces the photoemission from the TiO_2 surface is used to monitor the kinetic energy shift of the photoemission spectrum as a function of the pump−probe time delay.

For the pump−probe measurements, the IR-pump laser fluence is maintained at 5×10^9 W/cm^2 (10 mW, 25 fs, spot size of 1 mm). At this pump laser fluence a very small photoemission signal of a few counts per 1000 laser pulses is produced by the IR pump laser beam alone. This, however, clearly indicates that the pump laser pulse is producing multiphoton excitation, and most likely the excitation of both the direct and indirect band gaps of silicon is occurring at the pump laser fluences used in the present investigation.

In this work, transient signals have been recorded from the most relevant two cases, i.e., TiO_2 films with the lowest and the highest density of oxygen vacancies to monitor the charge carrier dynamics. In Figure 4 are displayed two transients

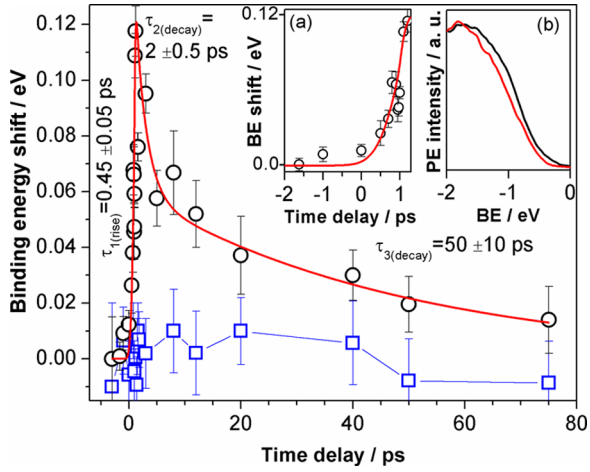

Figure 4. Transient shift of the photoemission spectra obtained from a defect-rich (open circles) and a defect-poor (open squares) 3 ML n-TiO_2 grown on p-Si(100) as a function of the pump−probe time delay. The open symbols represent the measured data while the red solid line is a fit to the measured data by an exponential rise followed by a double exponential decay convoluted with the instrumental time response function. For each data point, a photoemission spectrum is summed using 500 000 laser shots. Insets: (a) Rising region of the measured transient signal form the defect-rich p-TiO_2/p-Si(100). (b) Valence band photoemission in the binding energy (BE) range of 0 to −2 eV, recorded from a 3 ML n-TiO_2 film grown on the p-Si(100) substrate at a pump−probe delay time of −1 ps (red) and 1.5 ps (black).

DOI: 10.1021/acs.jpcc.5b11161
J. Phys. Chem. C 2016, 120, 2769−2776

recorded from defect-poor and defect-rich 3 ML TiO_2 films grown on the p-Si(100) substrate, in which the kinetic energy shift of the TiO_2 photoemission is plotted as a function of the pump−probe time delay. This shift can be clearly observed in the inset of Figure 4, which shows the valence band photoemission in the binding energy range of 0 eV to −2 eV, recorded from a 3 ML defect-rich n-TiO_2 film grown on the p-Si(100) substrate at pump−probe delay times of −1 and 1.5 ps. At negative time delay the XUV-probe laser pulse arrives at the sample surface before the IR-pump laser pulse, while at positive time delay the sequence of the laser pulses is exchanged, i.e., IR-pump is followed by the XUV-probe.

The defect-poor TiO_2 film is prepared by Ti evaporation on p-Si(100) at 575 K in an O_2 background pressure of 5.5×10^{-5} Torr. The defect-rich n-TiO_2 is prepared by Ti evaporation on p-Si(100) at room temperature in an O_2 background pressure of 7.5×10^{-9} Torr. The energy shift axis in Figure 4 is relative to the photoemission spectra recorded at negative time delays.

For each data point displayed in Figure 4, a photoemission spectrum is summed using 500 000 laser pulses. Due to the long time necessary to record a transient signal, the stability of the laser system and data acquisition reproducibility is checked by recording a reference spectrum at −3 ps pump−probe time delay after every two photoemission spectra. The errors obtained in the binding energy shifts are below ±15 meV. Moreover, to obtain these transient signals, the photoemission spectra are recorded with randomly distributed delays rather than in an ascending or a descending temporal sequence. The error bars in Figure 4 are obtained by calculating the standard deviation from two sets of measured data.

As mentioned above, the transient shift observed in the case of defect-rich n-TiO_2 film (cf. Figure 4) is attributed to an injection of electrons from the p-Si(100) substrate to the defect-rich n-TiO_2 layer due to the built-in electric field present in the space charge region of the n-TiO_2/p-Si(100) heterojunction. The electron injection from p-Si(100) to the defect-rich n-TiO_2 layer is expected to be energetically possible because the CBM of n-TiO_2 lies lower in energy than the states that are photoexcited by the pump laser pulse in the conduction band of p-Si(100). Due to the excess electrons that are present at the defect-rich n-TiO_2 surface, which act as a repelling potential for the photoemitted electrons, the photoemission spectrum at positive delay times is shifted to lower binding energies, i.e., higher kinetic energy, with respect to the spectrum recorded at negative delay time (cf. Figure 4).

In the case of defect-rich TiO_2/p-Si(100), an apparent transient signal is obtained. In this case, the transient signal rises from the zero time delay, reaches a maximum at 1.2 ps, and subsequently decays. The best fit to the measured data by an exponential rise followed by a double exponential decay convoluted with the instrumental time response function leads to a time constant of $\tau_{1(\text{rise})} = 450 \pm 50$ fs for the rise as well as a $\tau_{2(\text{decay})} = 2 \pm 0.5$ ps and a $\tau_{3(\text{decay})} = 50 \pm 10$ ps, for the decay (cf. Figure 4). The fast rise of the transient signal with a time constant of 450 fs is attributed to the ultrafast migration of electrons created in the space charge region of the p-Si(100) substrate to the defect-rich n-TiO_2 ultrathin film. A similar ultrashort transport time of 500 fs was measured in a pump−probe experiment on p-GaAs and attributed to the migration of electrons from the bulk to the sample surface.[21] The subsequent decay of the transient signal is due to the charge carrier recombination. Previous investigations have demonstrated that the charge carrier recombination at the surface of clean, defect-free silicon occurs within hundreds of nanoseconds.[22] The recombination time in the bulk of defect-poor TiO_2 occurs in hundreds of picoseconds.[23] Therefore, we consider that the recombination time constants (2 and 50 ps) obtained in the present experiments are strongly influenced by the presence of defect states in the TiO_2 layer. The fast decay of the transient signal with the time constant of 2 ps is attributed to the trapping of the charge carriers at the defect sites of n-TiO_2 accompanied by some recombination. The subsequent slow decay of the transient signal with the time constant of 50 ps is attributed to the charge carrier recombination at the surface of n-TiO_2. Because this recombination time constant of just 50 ps is much shorter than the one reported for a clean silicon surface or TiO_2 bulk, we consider that it is also affected by the defect states.

Recent femtosecond-transient absorption experiments performed by Sun et al. on undoped and doped TiO_2 films show that the charge recombination dynamics can be described, as in the present experiment, by a double exponential decay function.[23] The fast decay component obtained in the transient absorption experiments is attributed to charge carrier recombination that occurs because of the electron trapping at defect states located just below the CBM of TiO_2. The recombination time constant of 2−8 ps obtained in the transient absorption experiments decreases progressively as the doping concentration is increased. The slow decay component obtained in the transient absorption experiments in the case of an undoped TiO_2 sample is 471 ps and corresponds to charge carrier recombination in the bulk of the material. This time constant decreases to about 40 ps when the TiO_2 is doped, which clearly indicates that defect states decrease the charge recombination time. The results obtained in transient absorption experiments by Sun et al.[23] are in agreement with the results obtained in the present experiment.

Multiphoton excitation of the defect-rich n-TiO_2 layer by the IR-pump laser pulse is also possible. As revealed by the photoemission investigation shown in Figure 2, the energy of two or more IR-pump photons is necessary to excite electrons from the occupied defect states present in the band gap to the conduction band of the defect-rich n-TiO_2 (cf. Figure. 3). However, due to the limited number of atoms in the ultrathin n-TiO_2 layer, the number of charge carriers excited in TiO_2 is much smaller than the number of photoexcited charge carriers in p-Si(100), and consequently these charge carriers would have just a minor influence. Moreover, the excitation of an n-type semiconductor would lead to a surface photovoltage effect that would have an opposite result to the one observed in our experiment, i.e., holes are accelerated to the surface and electrons toward the bulk. However, this is not observed in our experiment, posssibly due to the small number of atoms of the TiO_2 layer.

As mentioned above, no transient signal is observed when defect-poor TiO_2 is grown on the p-Si(100) substrate (cf. Figure 4, squares). This can be attributed to the change of the energy band alignment at the TiO_2/Si(100) interface (cf. Figure 3) that reduces the built-in electric field across the space charge region of the TiO_2/Si(100) heterojunction and consequently leads to a reduction of the electron injection into the TiO_2/layer. As revealed by the photoemission spectra in Figure 2 and schematically represented in Figure 3, a shift in TiO_2 band structure to lower binding energies is observed as the number of oxygen vacancies in TiO_2 is reduced. This shift is in agreement with a reduction of the built-in electric field across

DOI: 10.1021/acs.jpcc.5b11161
J. Phys. Chem. C 2016, 120, 2769−2776

the space charge region of the TiO_2/Si(100) heterojunction.[19] Therefore, in the case of defect-poor TiO_2 film, even though the excited photoelectrons in Si have enough energy to overcome the barrier at the TiO_2/Si(100) heterojunction, they are not accelerated toward the TiO_2. Consequently, no electron accumulation at the surface and transient signal is observed in the case of defect-poor TiO_2.

4. CONCLUSIONS

Femtosecond-XUV photoemission spectroscopy was employed to investigate the electronic structure of defect-rich and defect-poor ultrathin TiO_2 films synthesized on a p-Si(100) substrate by Ti atoms evaporation in O_2 atmosphere. The concentration of oxygen vacancies was precisely tuned by controlling the oxygen background pressure during TiO_2 formation, as experimentally revealed through the photoemission yield of the occupied electronic states found in the band gap of TiO_2. The energetic location of these defect states is in excellent agreement with the theoretical predictions of Pacchioni and co-workers.[15] Using the pump−probe technique in conjunction with photoemission spectroscopy, the ultrafast transfer of electrons excited in p-Si(100) by an IR-pump laser pulse is observed in the defect-rich TiO_2 layer by the XUV-probe laser pulse that monitors the shift of the photoemission spectra due to the transient charging of the TiO_2 surface. The injection of the electrons from p-Si(100) into the TiO_2 layer occurs with a time constant of 450 fs. Subsequently, the charge recombination is best described by a double exponential decay function, in which the fast decay component with a time constant of 2 ps is attributed to electron trapping at defect states resulting in a rapid recombination there, which is in perfect agreement with the transient absorption data available in literature. The slow decay component with a time constant of 50 ps is attributed to the charge carrier recombination at the surface of TiO_2. No charge transfer is observed when defect-poor TiO_2 films are grown on the p-Si(100) substrate, most likely due to a decrease of the built-in electric field across the space charge region of the TiO_2/Si(100) heterojunction and consequently the reduction of the electron injection into the TiO_2 layer.

AUTHOR INFORMATION

Corresponding Author

*E-mail: srl@berkeley.edu. Fax: +1 510-643-1367. Tel: +1 510-643-5467.

Notes

The authors declare no competing financial interest.

ACKNOWLEDGMENTS

The authors gratefully acknowledge financial support provided by the U.S. Air Force Office of Scientific Research (Grant FA9550-14-1-0154). We thank Dr. Bill Flounders from Berkeley Marvell Nanofabrication Laboratory for providing the silicon substrate.

REFERENCES

(1) Wuerfel, P. *Physics of Solar Cells*; Wiley-VCH: Weinheim, 2005.
(2) Bauer, G. H. *Photovoltaic Solar Energy Conversion*; Springer: Berlin, 2015.
(3) Gardelis, S.; Nassiopoulou, A. G.; Manousiadis, P.; Vouroutzis, N.; Frangis, N. A silicon-wafer based p−n junction solar cell by aluminum-induced recrystallization and doping. *Appl. Phys. Lett.* **2013**, *103*, 241114.
(4) (a) Avasthi, S.; McClain, W. E.; Man, G.; Kahn, A.; Schwartz, J.; Sturm, J. C. Hole-blocking titanium-oxide/silicon heterojunction and its application to photovoltaics. *Appl. Phys. Lett.* **2013**, *102*, 203901-1−203901-4. (b) Jhaveri, J.; Avasthi, S.; Nagamatsu, K.; Sturm, J. C. Stable low-recombination n-Si/TiO_2 hole-blocking interface and its effect on silicon heterojunction photovoltaics. 2014 IEEE 40th Photovoltaic Specialist Conference (PVSC), 2014; pp 1525−1528. (c) Nagamatsu, K. A.; Avasthi, S.; Jhaveri, J.; Sturm, J. C. A 12% Efficient Silicon/PEDOT:PSS Heterojunction Solar Cell Fabricated at < 100 °C. *IEEE J. Photovolt.* **2014**, *4*, 260−264.
(5) Hummel, R. E. *Electronic Properties of Materials*, 3rd ed.; Springer-Verlag: New York, 2001.
(6) Kamat, P. V. Dominance of Metal Oxides in the Era of Nanotechnology. *J. Phys. Chem. Lett.* **2011**, *2*, 839−840.
(7) Seah, M. P.; Dench, W. A. Quantitative electron spectroscopy of surfaces. *Surf. Interface Anal.* **1979**, *1*, 2−11.
(8) Vaida, M. E.; Leone, S. R. Tracing dissociation dynamics of CH3Br in the 3Q0 state with femtosecond extreme ultraviolet ionization. *Chem. Phys.* **2014**, *442*, 41−47.
(9) Saathoff, G.; Miaja-Avila, L.; Aeschlimann, M.; Murnane, M. M.; Kapteyn, H. C. Laser-assisted photoemission from surfaces. *Phys. Rev. A: At., Mol., Opt. Phys.* **2008**, *77*, 022903-1−022903-16.
(10) Watts, J. F.; Wolstenholme, J. *An Introduction to Surface Analysis by XPS and AES*, 2nd ed.; Wiley: Chichester, 2003.
(11) Tass, Z.; Horvath, G.; Josepovits, V. K. Investigation of the titanium oxidation states by Auger electron spectroscopy. *Surf. Sci.* **1995**, *331*−*333*, 272−276.
(12) Perego, M.; Seguini, G.; Scarel, G.; Fanciulli, M.; Wallrapp, F. Energy band alignment at TiO_2/Si interface with various interlayers. *J. Appl. Phys.* **2008**, *103*, 043509.
(13) Jang, H. K.; Whangbo, S. W.; Kim, H. B.; Im, K. Y.; Lee, Y. S.; Lyo, I. W.; Whang, C. N.; Kim, G.; Lee, H.-S.; Lee, J. M. Titanium oxide films on Si(100) deposited by electron-beam evaporation at 250°C. *J. Vac. Sci. Technol., A* **2000**, *18*, 917−921.
(14) Kumarasinghe, A. R.; Flavell, W. R.; Thomas, A. G.; Mallick, A. K.; Tsoutsou, D.; Chatwin, C.; Rayner, S.; Kirkham, P.; Warren, S.; Patel, S.; Christian, P.; O'Brien, P.; Grätzel, M.; Hengerer, R. Electronic properties of the interface between p-CuI and anatase-phase n-TiO2 single crystal and nanoparticulate surfaces: A photoemission study. *J. Chem. Phys.* **2007**, *127*, 114703.
(15) Di Valentin, C.; Pacchioni, G.; Selloni, A. Reduced and n-Type Doped TiO2: Nature of Ti3+ Species. *J. Phys. Chem. C* **2009**, *113*, 20543−20552.
(16) Onda, K.; Li, B.; Petek, H. Two-photon photoemission spectroscopy of Ti O2 (110) surfaces modified by defects and O2 or H2 O adsorbates. *Phys. Rev. B: Condens. Matter Mater. Phys.* **2004**, *70*, 045415.
(17) Jhaveri, J.; Avasthi, S.; Man, G.; McClain, W. E.; Nagamatsu, K.; Kahn, A.; Schwartz, J.; Sturm, J. C. Hole-blocking crystalline-silicon/titanium-oxide heterojunction with very low interface recombination velocity. 2013 IEEE 39th Photovoltaic Specialists Conference (PVSC), 2013; pp 3292−3296.
(18) Kittel, C. *Introduction to Solid State Physics*; John Wiley & Sons: New York, 1976.
(19) (a) Colinge, J.-P.; Colinge, C. A. *Physics of Semiconductor Devices*; Springer: New York, 2006. (b) Sze, S. M.; Ng, K. K. *Physics of Semiconductor Devices*, 3rd ed.; John Wiley and Sons: Hoboken, NJ, 2007.
(20) Van Ruyven, L. J. Phenomena at Heterojunctions. *Annu. Rev. Mater. Sci.* **1972**, *2*, 501−528.
(21) Siffalovic, P.; Drescher, M.; Heinzmann, U. Femtosecond time-resolved core-level photoelectron spectroscopy tracking surface photovoltage transients. *Europhys. Lett.* **2002**, *60*, 924−930.
(22) Spencer, B. F.; Graham, D. M.; Hardman, S. J. O.; Seddon, E. A.; Cliffe, M. J.; Syres, K. L.; Thomas, A. G.; Stubbs, S. K.; Sirotti, F.; Silly, M. G.; Kirkham, P. F.; Kumarasinghe, A. R.; Hirst, G. J.; Moss, A. J.; Hill, S. F.; Shaw, D. A.; Chattopadhyay, S.; Flavell, W. R. Time-resolved surface photovoltage measurements at n-type photovoltaic

DOI: 10.1021/acs.jpcc.5b11161
J. Phys. Chem. C 2016, 120, 2769−2776

surfaces: Si(111) and ZnO(1010). *Phys. Rev. B: Condens. Matter Mater. Phys.* **2013**, *88*, 195301-1−195301-16.
(23) Sun, J.; Yang, Y.; Khan, J. I.; Alarousu, E.; Guo, Z.; Zhang, X.; Zhang, Q.; Mohammed, O. F. Ultrafast Carrier Trapping of a Metal-Doped Titanium Dioxide Semiconductor Revealed by Femtosecond Transient Absorption Spectroscopy. *ACS Appl. Mater. Interfaces* **2014**, *6*, 10022−10027.

DOI: 10.1021/acs.jpcc.5b11161
J. Phys. Chem. C 2016, 120, 2769−2776